

Spatial noise correlations of a chain of ultracold fermions - A numerical study

Andreas Lüscher and Andreas M. Läuchli

Institut Romand de Recherche Numérique en Physique des Matériaux (IRRMA), EPFL, CH-1015 Lausanne, Switzerland

Reinhard M. Noack

Fachbereich Physik, Philipps-Universität Marburg, D-35032 Marburg, Germany

(Dated: October 31, 2021)

We present a numerical study of noise correlations, i.e., density-density correlations in momentum space, in the extended fermionic Hubbard model in one dimension. In experiments with ultracold atoms, these noise correlations can be extracted from time-of-flight images of the expanding cloud. Using the density-matrix renormalization group method to investigate the Hubbard model at various fillings and interactions, we confirm that the noise correlations contain full information on the most important fluctuations present in the system. We point out the importance of the sum rules fulfilled by the noise correlations and show that they yield nonsingular structures beyond the predictions of bosonization approaches. Noise correlations can thus serve as a universal probe of order and can be used to characterize the many-body states of cold atoms in optical lattices.

PACS numbers: 03.75.Ss, 03.75.Mn, 42.50.Lc

I. INTRODUCTION

Recent advances in methods for trapping and controlling ultracold atoms have opened up the promising possibility of directly simulating strongly interacting many-body Hamiltonians. These experimental systems can be used to engineer and analyze models that lie beyond the scope of present analytical and numerical methods, thus potentially shedding new light on fundamental quantum many-body problems [1, 2, 3, 4, 5] such as the nature of the mechanism for high- T_c superconductivity or whether a true spin liquid can be realized. Such systems can be formed by trapping atomic gases in one-, two-, or three-dimensional optical lattices. The interactions can be accurately tuned by adjusting external fields. In a similar spirit, it has recently been proposed to simulate strongly correlated systems in experiments by studying the dynamics of polaritons in arrays of electromagnetic cavities, see Ref. 6.

The techniques for manipulating ultracold atoms are fairly advanced and have already enabled a broad range of astonishing systems, such as a superfluid, a Mott insulator [7, 8], a strongly interacting Fermi gas [9] or also mixtures of bosonic and fermionic gases [10]. However, the subsequent analysis of their properties has proven to be difficult. In view of the application to solid state problems, it is crucial to have tools at hand that can accurately describe the engineered state, preferably by extracting the correlation functions of the atomic gas. A recent proposal [11] for a universal probe of correlations suggested measuring the shot noise in time-of-flight images of the expanding cloud of atoms after release from the trap. This method is based on the fact that, after a long enough time of flight t , the density distribution of the expanding cloud becomes proportional to the momentum distribution in the interacting system [11, 12],

$$\langle n(\mathbf{r})_t \rangle \propto \frac{m}{\hbar t} \langle n_{\mathbf{q}(r)} \rangle ,$$

with momentum $\mathbf{q}(\mathbf{r}) = m\mathbf{r}/(\hbar t)$ for an atom of mass m . The noise in the image-by-image statistics is governed by higher order correlations of the initial state

$$G_{\sigma\sigma'}(\mathbf{r}, \mathbf{r}') = \langle n_{\mathbf{q}(r)} n_{\mathbf{q}(r')} \rangle - \langle n_{\mathbf{q}(r)} \rangle \langle n_{\mathbf{q}(r')} \rangle , \quad (1)$$

where σ is an internal quantum number, e.g., the spin, that allows different states to be distinguished. By analyzing the shot noise in several mean-field states, Altman *et al.* [11] showed that the presence of a particular order leaves a very distinctive fingerprint on the noise correlations, e.g., due to superconductivity or spin order. On the experimental side, this quantity has already been measured on several occasions, in both fermionic and bosonic cold atomic gases, i.e., in bosonic Mott insulators [13, 14], fermionic superfluids [15], and band insulators [16].

In the following, we will treat one-dimensional (1D) fermionic systems on an optical lattice and will concentrate on the noise correlations of the lattice model itself:

$$G_{\sigma\sigma'}(k, k') = \langle n_{k,\sigma} n_{k',\sigma'} \rangle - \langle n_{k,\sigma} \rangle \langle n_{k',\sigma'} \rangle ,$$
$$G(k, k') = \sum_{\sigma,\sigma'} G_{\sigma\sigma'}(k, k') . \quad (2)$$

Here the brackets denote the ground state expectation value. Shortly after the pioneering analysis of Ref. 11, which was based on mean-field calculations, Mathey *et al.* [17] analyzed the shot noise for a 1D Tomonaga-Luttinger (TL) liquid within a bosonization approach, allowing them to explore the momentum-dependence around opposite Fermi points, i.e., around $k \approx k_F$ and $k' \approx -k_F$. In these TL liquids, different types of order compete, leading to a rich structure in the noise correlations. In the present paper, we employ the density-matrix renormalization group (DMRG) method [18, 19] to study the noise correlations in the 1D extended Hubbard model. This numerical approach allows us to go beyond the Luttinger theory and to uncover the full set of features that are contained in the noise correlations

within the entire Brillouin zone. In the vicinity of opposite Fermi points, we find perfect agreement with the analytical predictions of Ref. 17.

The remainder of the paper is organized as follows: In Sec. II, we discuss general properties of noise correlations, independent of the microscopic model. The extended Hubbard model considered in this work is then introduced in Sec. III, together with a summary of the different (quasi-)orders encountered in our numerical approach. Our main results, the analysis of the noise correlations for different phases of the extended Hubbard model, are presented in Sec. IV. In Sec. V, we make the connection to atomic physics and discuss experimental issues. We present our conclusions in Sec. VI.

II. PROPERTIES OF NOISE CORRELATIONS IN FERMIONIC LATTICE MODELS

Before considering a specific microscopic model, it is useful to discuss several general properties of the noise correlation functions at the lattice level. In the following, we consider the noise correlations (2) on a periodic lattice with L sites. In this case, k denotes the lattice momentum and σ describes an internal quantum number that we associate with the spin, i.e., $\sigma \in \{\uparrow, \downarrow\}$. In general, σ can denote a more general flavor or species index; the statements below remain valid as long as the density operator

$$n_{k,\sigma} = c_{k,\sigma}^\dagger c_{k,\sigma}$$

can be written as a product of creation and annihilation operators that satisfy the canonical fermionic commutation rules

$$\begin{aligned} \{c_{k,\sigma}, c_{k',\sigma'}\} &= \{c_{k,\sigma}^\dagger, c_{k',\sigma'}^\dagger\} = 0, \\ \{c_{k,\sigma}, c_{k',\sigma'}^\dagger\} &= \delta_{k,k'} \delta_{\sigma,\sigma'}. \end{aligned}$$

It is convenient to use the Fourier transformation

$$c_{k,\sigma} = \frac{1}{\sqrt{L}} \sum_l e^{ikl} c_{l,\sigma}, \quad (3)$$

so that the creation and annihilation operators in coordinate space also obey the standard commutation relations. Under these assumptions, G satisfies the following exact statements:

1. *Bounds:* For all k, k' and σ, σ' , G is uniformly bounded

$$|G_{\sigma\sigma'}(k, k')| \leq \frac{1}{4}, \quad (4)$$

independent of the system size, i.e., $G_{\sigma\sigma'}(k, k')$ itself cannot diverge with system size.

2. *Sum rules:* In a system in which the number of particles of every species is conserved, the noise correlations satisfy the sum rule

$$\sum_{k,k'} G_{\sigma\sigma'}(k, k') = \langle N_\sigma N_{\sigma'} \rangle - \langle N_\sigma \rangle \langle N_{\sigma'} \rangle = 0, \quad (5)$$

where $N_\sigma = \sum_k n_{k,\sigma}$.

3. *Equal-spin momentum diagonal:* Along the momentum diagonal $k = k'$, the equal spin $\sigma = \sigma'$ shot noise is given by

$$G_{\sigma\sigma}(k, k) = \langle n_{k,\sigma} \rangle - \langle n_{k,\sigma} \rangle^2 \geq 0. \quad (6)$$

This part of the noise correlation function is therefore completely determined by the momentum distribution function $\langle n_{k,\sigma} \rangle$ itself and does *not* contain any other information.

The basic idea behind the use of density-density correlations as a universal probe of the system lies in the simple fact that they contain important parts of various particle-hole *and* particle-particle correlation functions. Quite generally, a particle-hole scattering operator with net momentum q and form factor $f(k)$ can be written as

$$\mathcal{O}_{\text{p-h}}^\dagger(f, q) = \frac{1}{\sqrt{L}} \sum_{k,\alpha,\beta} f(k)_{\alpha\beta} c_{k+q,\alpha}^\dagger c_{k,\beta}, \quad (7)$$

with

$$f(k)_{\alpha\beta} = \begin{cases} f^{\text{CDW}}(k) \delta_{\alpha\beta} \\ \frac{1}{2} \mathbf{f}^{\text{SDW}}(k) \cdot \boldsymbol{\sigma}_{\alpha\beta} \end{cases},$$

for generalized charge-density waves (CDW) and spin-density waves (SDW), respectively [20]. Here $\boldsymbol{\sigma}$ are the Pauli matrices. This ensemble of CDW and SDW operators encompasses a large variety of particle-hole instabilities, such as conventional charge and spin-density waves, bond-order waves, staggered flux phases, as well as spin nematic states [20]. In 1D fermionic systems, the strongest instabilities in the particle-hole sector often occur at $q = 2k_F$. However, in some cases, the $q \rightarrow 0$ correlations can also become strong, for example, close to a ferromagnetic transition, or when longer-range interactions induce important correlations at wave vectors different from $2k_F$. Analogously, in the particle-particle sector, a scattering operator of particle pairs with total momentum q and form factor f reads

$$\mathcal{O}_{\text{p-p}}^\dagger(f, q) = \frac{1}{\sqrt{L}} \sum_{k,\alpha,\beta} f(k)_{\alpha\beta} c_{-k+q,\alpha}^\dagger c_{k,\beta}^\dagger. \quad (8)$$

Here the dependence of the form factor on the spin indices α, β determines whether the operator describes spin-singlet (SS) or spin-triplet (TS) superconducting pairing. In the case of SS, f is an even function in the momentum k , whereas for TS, f is odd in k . In the following, we restrict our discussion to the most common case of pairs with total momentum $q = 0$, but we remark that the Fulde-Ferrell-Larkin-Ovchinnikov (FFLO) [21] state appearing in the current discussion on the superfluid pairing properties in population-imbalanced Fermi gases would require a finite q .

The strongest correlations can be identified by comparing the structure factors of possible competing orderings.



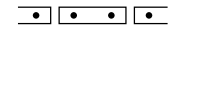


Case	Couplings ($t=1$)	x	LRO	QLRO	Strong-coupling limit
IV A	$U=10, V=10$	1/2	CDW	–	
IV B	$U=10$	1/2	–	SDW,pCDW	
IV C	$U=10, t'=0.7$	1/2	pCDW	–	
IV D	$U=10, V=10$	1/4	CDW ($4k_F$)	SDW	
IV E	$U=-10$	3/8	–	SS [CDW]	
IV F	$U=10$	3/8	–	SDW,CDW [SS,TS]	

TABLE I: Dominant correlations for the parameter sets studied in this work, supplemented with schematic pictures of the ground states. LRO stands for true long-range order, while QLRO denotes algebraic correlations (quasi-long-range order). We encounter charge-density waves (CDW), spin-density waves (SDW), bond-order waves (pCDW, where the kinetic energy is modulated), singlet superconductivity (SS) and triplet superconductivity (TS). The brackets indicate the subdominant correlation functions, i.e., ones which decay with a faster power law than the dominant correlations. The momentum of the particle-hole correlations is $2k_F = 2\pi x$, unless stated otherwise. The pairing correlations are for pairs with zero total momentum.

With the above definitions of the scattering operators, the associated structure factors can be expressed as

$$S_\xi(f, q) = \left\langle \mathcal{O}_\xi^\dagger(f, q) \mathcal{O}_\xi(f, q) \right\rangle. \quad (9)$$

In the case of true long-range order, the structure factor taken at the ordering wave vector k would grow linearly with the system size and would thus diverge in the thermodynamic limit. For the quasi-long-range order encountered in many 1D systems, in which the asymptotic decay of the correlation functions has the form of a power law (algebraic decay), the corresponding structure factors can show similar power-law divergences, with exponents that depend on the value of the interactions in the microscopic model. To see the tight correspondence between the structure factor (9) and the noise correlation function (2), it is illuminating to rewrite the operators in a slightly different way. For instance, the four-body operators of the particle-hole structure factor that contribute to the noise correlations read

$$\begin{aligned} f(k)_{\alpha\beta}^* f(k')_{\alpha'\beta'} c_{k+q,\alpha}^\dagger c_{k,\beta} c_{k',\beta'}^\dagger c_{k'+q,\alpha'} \Big|_{\substack{k'=k \\ \alpha=\alpha' \\ \beta=\beta'}} \\ = -|f(k)_{\alpha\beta}|^2 c_{k,\beta}^\dagger c_{k,\beta} c_{k+q,\alpha}^\dagger c_{k+q,\alpha} + \dots, \end{aligned}$$

where the expression on the second line is easily recognized as one term of the noise correlations. The additional terms are two-body operators that arise due to commutation rules. From this “identification”, we draw three important conclusions: First, only the modulus of the form factors $f(k)$ enters the noise correlations. Two types of order that differ only by a phase factor are thus difficult to distinguish by inspecting only the vicinity of

the Fermi points. For instance, a bond-order-wave state, i.e., a bond-centered CDW with p -wave character, and a conventional site-centered s -wave CDW lead to similar features in the shot noise. Second, since the noise correlations are bounded by Eq. (4), they cannot diverge. However, we expect any divergences present in the structure factors, properly rescaled, to also appear in the rescaled noise correlations LG , where L is the size of the system; see also Ref. 17. Third, it is interesting to note that only the nature of a fluctuation, i.e., whether it is particle-hole or particle-particle-like, determines the sign of the divergence. According to the analysis above, particle-hole correlations enter with a negative sign as dips along $k' = k \pm q$, while particle-particle fluctuations give a positive contribution and are observed along the anti-diagonal $k' = -k$ of the shot noise. This is what is expected intuitively because a particle-hole scattering process is only effective if the k -orbital is occupied in a different way than the $k \pm q$ -orbital, i.e., if they are anticorrelated. On the other hand, for particle-particle scattering, the k and the $-k$ -orbitals must be both filled or both empty in order to be effective, i.e., they must be (positively) correlated.

III. THE EXTENDED HUBBARD MODEL

We now consider the extended Hubbard model on a chain with L sites and periodic boundary conditions

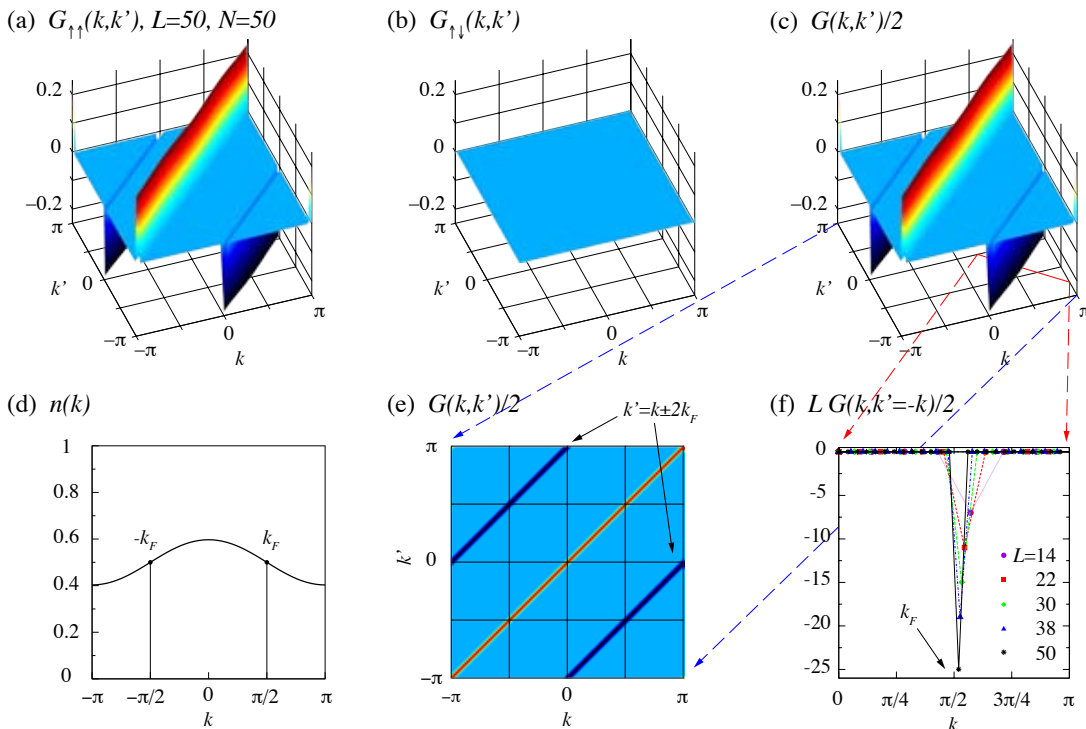


FIG. 1: (Color online). Noise correlations (a, b, c, e, f) and momentum distribution (d) in the extended Hubbard chain with $U/t = V/t = 10$ at filling $x = 1/2$, i.e., $k_F = \pi/2$, obtained using coordinate-space DMRG calculations and subsequent Fourier transformation. The system exhibits an ordered $2k_F$ -CDW, manifesting itself in the pronounced dip along $k' = k \pm 2k_F$ in $G_{\uparrow\uparrow}$ (a) and vanishing correlations in the $\uparrow\downarrow$ -channel (b). This can be best seen in the intensity plot of the total noise correlations (e). The rescaled shot noise (f) at $k = k_F$, $k' = -k_F$ scales linearly with the size of the system L , indicating true long-range order. Note that because of the closed shell configurations used in these calculations, k_F is not part of the discrete Brillouin zone. The finite-size scaling (f) thus shows paths along $k' = -k + 2\pi/L$.

(PBC). The Hamiltonian of this system reads

$$H = -t \sum_{l,\sigma} \left(c_{l,\sigma}^\dagger c_{l+1,\sigma} + \text{H.c.} \right) + U \sum_l n_{l,\uparrow} n_{l,\downarrow} - t' \sum_{l,\sigma} \left(c_{l,\sigma}^\dagger c_{l+2,\sigma} + \text{H.c.} \right) + V \sum_l n_l n_{l+1}, \quad (10)$$

where $c_{l,\sigma}^\dagger$ ($c_{l,\sigma}$) creates (destroys) an electron with spin σ on site l , $n_{l,\sigma} = c_{l,\sigma}^\dagger c_{l,\sigma}$ is the occupation number operator and the parameters t' , U and V characterize the next-nearest-neighbor hopping, the on-site and the nearest-neighbor interactions, respectively. We focus on the ground state sector with $N_\uparrow = N_\downarrow = N/2$, with N the total number of particles. The filling x is defined as $x = N/(2L)$ and thus, as usual, half-filling ($x = 1/2$) corresponds to one electron per site on average. For convenience, we set the hopping amplitude $t = 1$ and express the other interactions in units of t . The extended Hubbard model is $SU(2)$ -invariant for all values of the couplings, and the ground state is a spin singlet for the parameter values considered in this work. Longitudinal and transverse spin correlations, which appear in $G_{\uparrow\uparrow}$ and $G_{\uparrow\downarrow}$, respectively, are therefore identical by symmetry. Furthermore, the continuous $U(1)$ gauge symmetry

and the $SU(2)$ spin invariance forbid the appearance of true superconducting or spin-ordered states in this 1D model. However, the discrete lattice symmetries or the time-reversal symmetry can, in principle, be broken, giving rise to commensurate charge-density or bond-order waves.

For the generic case of repulsive interactions and incommensurate fillings, the low-energy sector of the extended Hubbard model is accurately described as a TL liquid [32] with four independent parameters that completely specify the model: the velocities of the charge and spin excitations, v_ρ and v_σ , respectively, and the correlation exponents K_ρ and K_σ . Since the $SU(2)$ symmetry of the extended Hubbard model implies $K_\sigma = 1$, the asymptotic behavior of the correlation functions depends only on K_ρ , which in terms depends on the interactions and the filling. In the absence of interactions, these velocities reduce to the Fermi velocity v_F , and the correlation exponents are equal to 1.

The Hamiltonian (10) has been studied extensively in the past (see, e.g., Ref. 22 for an overview). Based on this knowledge, we have chosen a few interesting parameter sets in the global phase diagram [23, 24, 25, 26, 27, 28, 29] to investigate the noise correlations, see Tab. I. The presentation in Sec. IV is ordered according to increasing

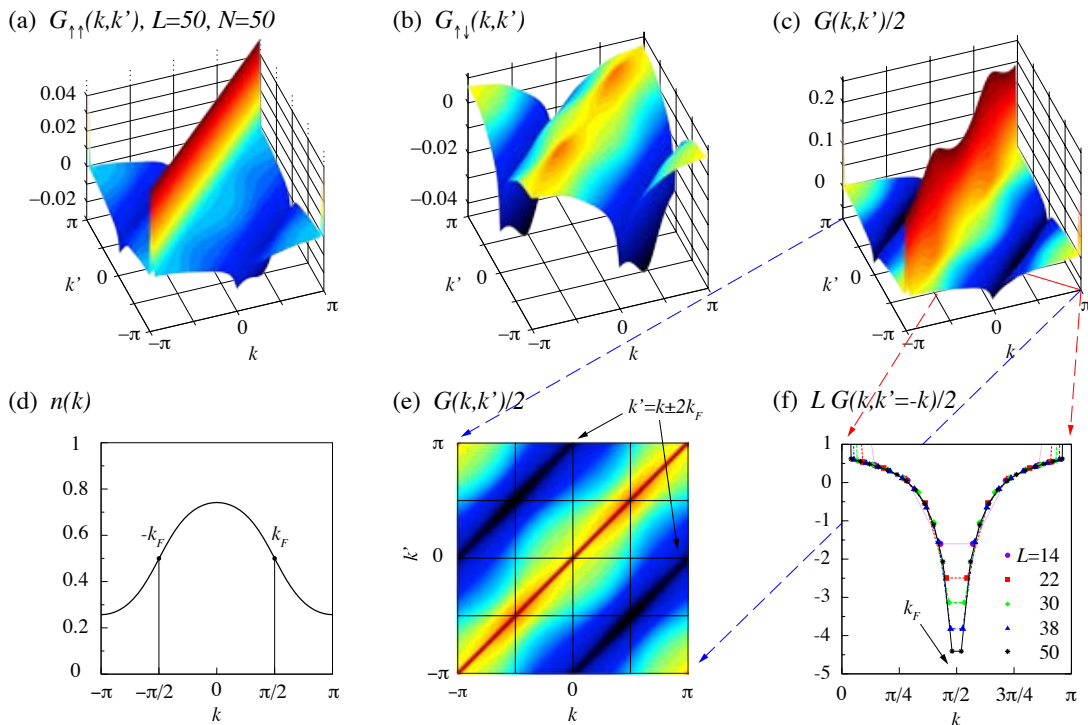


FIG. 2: (Color online). Noise correlations (a, b, c, e, f) and momentum distribution (d) for the Hubbard chain with $U/t = 10$ and $V = 0$ at half-filling, i.e., $k_F = \pi/2$. The system is in the Heisenberg regime where only spin-spin correlations are critical because the charge sector is gapped. Note that in (a), we have chosen a very small upper cutoff to reveal the structure around opposite Fermi points. The behavior along the diagonal can be deduced from (c). The system exhibits a $2k_F$ -SDW, which manifests itself in both the $\uparrow\uparrow$ (a) and the $\uparrow\downarrow$ -channel (b) as dips along $k' = k \pm 2k_F$. This is well visible in the intensity plot (e). In contrast to the case of Fig. 1, this system only exhibits quasi long-range order. The rescaled shot noise (f) thus grows much more slowly than in the case of true long-range order.

complexity of the noise spectrum.

IV. NUMERICAL RESULTS

In this section, we present our numerical results for the noise correlations G (2) in the extended Hubbard chain (10) obtained by DMRG calculations in coordinate space and exact diagonalizations (ED) in momentum space [30]. Due to the vast number $[\mathcal{O}(L^4)]$ of four-point correlation functions that have to be evaluated in a coordinate space approach, we only consider chains with up to 56 sites. These sizes are, however, sufficient for the purpose of the present work because the main features of the noise correlations are already well-established in these systems and because the finite-size scaling does not show any ambiguities. We have checked the implementation and the accuracy of the coordinate-space DMRG calculations against ED results on smaller samples (up to $L = 20$ sites) and have found very good agreement. In addition, our calculations all comply very well with the sum rule (5).

The number of fermions N and the system size L are always chosen so that *closed shell*, configurations occur, i.e., so that all orbitals below k_F are occupied, while or-

bitals above k_F are empty. This condition translates into a fermion number $N = 2 + 4m$, where m is a nonnegative integer and hence $L = N/(2x)$. On the one hand, this choice eliminates spurious effects arising from open-shell conditions, but, on the other hand, the Fermi vector k_F cannot be part of the discrete Brillouin zone; only even multiples of it can be resolved. Nevertheless, the effects we will study will be well-visible in the vicinity of the Fermi momentum; its behavior for $k \rightarrow \pm k_F$ can easily be deduced.

A. Ordered charge-density wave

Let us start with a simple case that exhibits true long-range order by choosing a half-filled system ($x = 1/2$) with $U/t = 10$ and $V/t = 10$. In this case, the charge and the spin sectors are gapped. In the limit $t = 0$, $V/2 > U$ is a sufficient condition for the existence of a charge-density-wave state in which every second site is doubly occupied, see Tab. I. In this strong-coupling limit, the noise correlations can be calculated analytically using

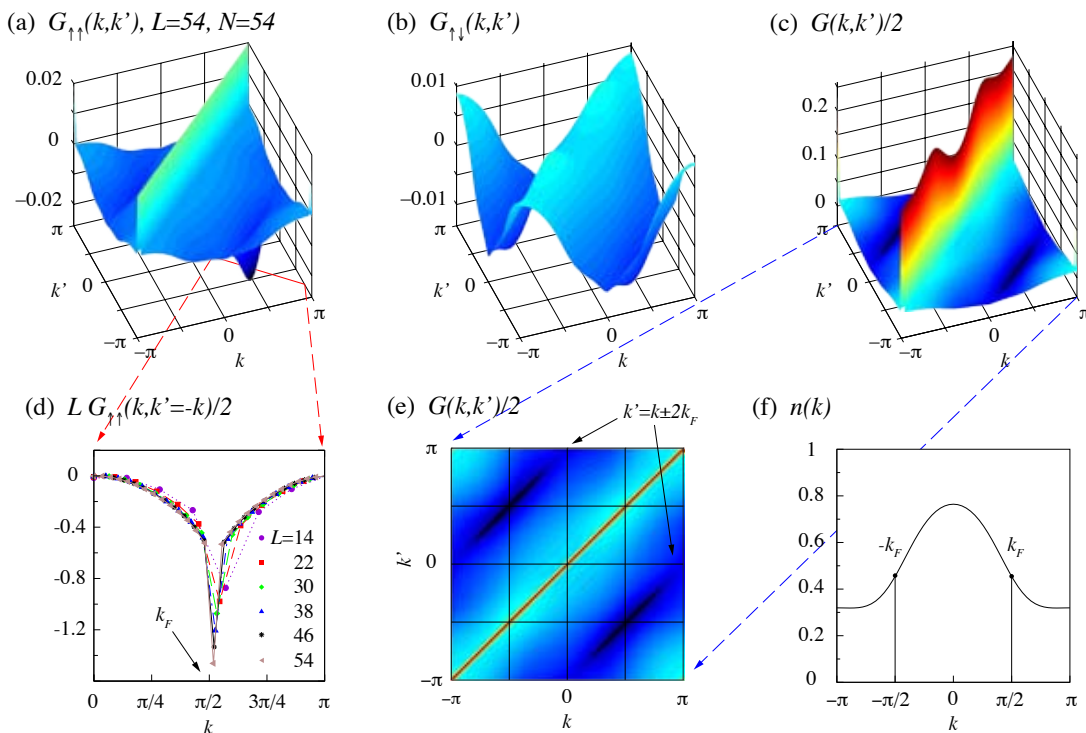


FIG. 3: (Color online). Noise correlations (a, b, c, d, e) and momentum distribution (f) in the Hubbard chain with $U/t = 10$, $t'/t = 0.7$, and $V = 0$ at filling $x = 1/2$. The system is in a phase with long-range modulations of the kinetic energy. In $G_{\uparrow\uparrow}$, (a), a rather sharp dip along $k' = k \pm \pi$ can be seen. The finite-size scaling (d) illustrates the long-range character of the correlations. Note that because of the closed shell configurations used in these calculations, k_F is not part of the discrete Brillouin zone. The finite-size scaling (d) thus shows paths along $k' = -k + 2\pi/L$. In the $\uparrow\downarrow$ -channel (b), only a shallow valley can be identified along the diagonal $k' = k \pm \pi$. Finite-size scaling (not shown) indicates that these spin correlations are short-range. Due to the phase insensitivity, the noise correlations alone cannot distinguish between this bond-centered and a conventional site-centered CDW, when focussing only on a close neighborhood of the Fermi points.

a site-factorized wave function

$$\begin{aligned}
 G_{\uparrow\uparrow}(k, k' \neq k) &= -\frac{1}{L^2} \sum_{l=1}^{L/\mu} \sum_{l'=1}^L e^{i(k-k')(l-l')} \delta_{l', l+m\mu} \\
 &\approx -\frac{1}{\mu^2} \delta_{k', k \pm \frac{2\pi}{\mu}}, \\
 G_{\uparrow\downarrow}(k, k') &= 0.
 \end{aligned} \tag{11}$$

Here μ is the period of the modulation and m an integer. We thus expect a signature along $k' = k \pm 2\pi/\mu$.

These arguments are in perfect quantitative agreement with the numerical results for the shot noise shown in Fig. 1, which clearly reveal a $2k_F = \pi$ CDW signature in the $\uparrow\uparrow$ -channel and vanishing correlations in the $\uparrow\downarrow$ -channel. Although the featureless momentum distribution shown in Fig. 1(e) is an indicator of a gapped state, it does not reveal its nature. Since we have chosen the number of particles and the length of the chain to exclude the Fermi points, a slice along the anti-diagonal $k' = -k$ does not contain the minimum of the dip. However, along a slightly shifted path along $k' = -k + 2\pi/L$, as depicted in Fig. 1(f), it is easy to see that the minimum of the rescaled shot noise increases linearly with the size of the system, in agreement with the strong-coupling derivation

above. In the thermodynamic limit, the rescaled shot noise thus contains a diverging dip along $k' = k \pm 2k_F$.

B. Algebraically decaying spin-density wave

Without the nearest-neighbor interaction V , one recovers the standard Hubbard chain. At half-filling, the charge sector is gapped, but the spin excitations are gapless. In this case, the correlation exponent K_ρ vanishes and density-density correlations decay exponentially. Because of the $SU(2)$ invariance, $K_\sigma = 1$ and the spin-spin correlations are critical, asymptotically decaying as $1/r$. The low-energy sector of a half-filled Hubbard model is equivalent to a $S = 1/2$ Heisenberg chain. A snapshot of a spin configuration is depicted in Tab. I. The simple analytical strong-coupling analysis above is equally applicable to spin modulations; the only difference is that spin correlations enter not only $G_{\uparrow\uparrow}$, but also $G_{\uparrow\downarrow}$. The periodicity of the modulation is again two lattice spacings, leading to a signal along $k' = k \pm 2k_F$. In contrast to the previous case, this system does not exhibit true long-range order because the SDW state would break a continuous symmetry. The ordering tendencies are ac-

cordingly less distinct than in the CDW example with true long-range order. This is illustrated in the finite-size scaling analysis of the rescaled shot noise LG in Fig. 2(f).

In addition to the well-known staggered spin correlations, the Heisenberg chain also has staggered dimer-dimer correlations decaying with the same power law (disregarding logarithmic corrections). In fermionic language, these dimer correlations share the same properties as the bond-order-wave correlations, i.e., are modulations of the kinetic energy. In terms of higher angular momentum density waves, this is a p -wave CDW. We therefore see a superposition of both the spin and the kinetic energy correlations in $G_{\uparrow\uparrow}$ along $k' = k \pm 2k_F$.

C. Ordered bond-order wave (dimerized) state

To extend the discussion on critical bond-order wave correlations in the half-filled Hubbard model, it is interesting to separate the two contributions by driving the system into a dimerized phase, where the kinetic energy is modulated and the spin-spin correlations decay exponentially. Such a phase has been reported in Ref. 29, in a study of the Hubbard model ($V = 0$) with an additional next-nearest neighbor hopping t' , where a spin gap opens and the spin correlations become very short-range. In the large U limit, this model maps onto a frustrated Heisenberg chain, which is known to be dimerized at the Majumdar-Ghosh point $J_2/J_1 = 1/2$ [31]. In Ref. 29, it has been shown that this phase persists for finite values of U . We have therefore chosen to investigate the noise correlations for a half-filled chain with $U/t = 10$ and $t'/t = 0.7$. In a state where the kinetic energy is modulated with period μ , we expect pronounced correlations of the form

$$\left\langle \left(c_{i,\sigma}^\dagger c_{i+1,\sigma} + \text{H.c.} \right) \left(c_{i+\mu,\sigma'}^\dagger c_{i+\mu+1,\sigma'} + \text{H.c.} \right) \right\rangle .$$

Tab. I depicts such a dimerized state (with modulation period $\mu = 2$ lattice spacings) schematically. Writing the noise correlations (2) in coordinate space, one can convince oneself (after a bit of algebra) that a bond-order wave leaves a non-trivial fingerprint only in the $\uparrow\uparrow$ -channel along $k' = k \pm \pi$. Due to the particle-hole nature of the fluctuation, the signature is negative. The $\uparrow\downarrow$ -channel contains non-singular contributions of the form $e^{\pm ik} e^{\pm ik'}$. This crude approximation is confirmed by our numerical results presented in Fig. 3. The well-pronounced dip along $k' = k \pm \pi$ in $G_{\uparrow\uparrow}$ is clearly distinguishable from the shallow surface in $G_{\uparrow\downarrow}$. The finite-size scaling [Fig. 3(d)] illustrates the long-range character of the correlations. In contrast, the finite-size scaling of $G_{\uparrow\downarrow}$ along the same path (not shown) quickly saturates, showing that the spin correlations are indeed short-range. Note that the noise correlations alone cannot distinguish between this bond-centered and a conventional site-centered CDW in 1D due to the phase insensitivity.

D. Ordered charge-density wave coexisting with an algebraically decaying spin-density wave

Another interesting example is a system with both SDW quasi-order and true long-range CDW ordering at different wave vectors, realized for a quarter-filled chain with $U/t = V/t = 10$. For these parameters, the model is an insulator with a charge gap, i.e., the correlation exponent $K_\rho = 0$. As will be given explicitly in Eqs. (12), the spin-spin correlations decay as $1/r$, as in the case of the Heisenberg chain. The strong-coupling ground state is shown in Tab. I. Based on this picture, we expect $2k_F$ spin modulations and $4k_F$ charge modulations to be present. This prediction is in excellent agreement with the numerical results of Fig. 4. A pronounced CDW response is visible along $k' = k \pm \pi$ in $G_{\uparrow\uparrow}$ [Fig. 4(a)], while less pronounced SDW ordering can be identified in $G_{\uparrow\uparrow}$ and $G_{\uparrow\downarrow}$ [Fig. 4(b)] along $k' = k \pm \pi/2$. Note that the small dips along $k' = k \pm 3\pi/2$ in Fig. 4(b) are just due to the periodicity of the Brillouin zone. The finite-size scaling along the anti-diagonal clearly reveals that charge ordering is much stronger than the tendency to form a SDW, as can be seen in Fig. 4(f).

E. Algebraically decaying singlet superconductivity and charge-density wave correlations

For an attractive on-site interaction ($U/t < 0$), the fermions tend to pair in singlets, leading to a gap in the spin sector, i.e., it requires a finite energy to break up an on-site pair because, even in the thermodynamic limit, spin correlations and triplet superconducting correlations decay exponentially, while singlet superconducting and charge fluctuations exhibit an asymptotic behavior of the form [23]

$$C_{SS}(l) = \langle c_{l,\uparrow}^\dagger c_{l,\downarrow}^\dagger c_{0,\downarrow} c_{0,\uparrow} \rangle \rightarrow \frac{A_{SS}}{|l|^{1/K_\rho}} ,$$

$$C_{CDW}(l) = \langle n_l n_0 \rangle \rightarrow n^2 + A_{CDW} \frac{\cos(2k_F l)}{|l|^{K_\rho}} ,$$

with amplitudes A_ξ that depend on the values of the interactions and on the filling. The presence of a spin gap is taken into account by formally setting the correlation exponent $K_\sigma \rightarrow 0$. Since $K_\rho > 1$ for attractive interactions and away from half filling, the SS fluctuations are always dominant and the tendency to form a CDW is subdominant. Fig. 5 shows the noise correlations and the momentum distribution [Fig. 5(d)] calculated for a Hubbard model with attractive interaction $U/t = -10$ ($V = 0$) at a filling of $x = 3/8$. Based on Ref. 22, we estimate $K_\rho \approx 1.3$. Note that in Fig. 5(a), we have chosen a very small cutoff in order to display the much smaller CDW signature along $k' = k + 2k_F$ in $G_{\uparrow\uparrow}$. As expected, SS correlations are visible along the anti-diagonal in $G_{\uparrow\downarrow}$ and clearly dominate over the CDW signature; this is evident in the total shot noise, Fig. 5(c). In the region acces-

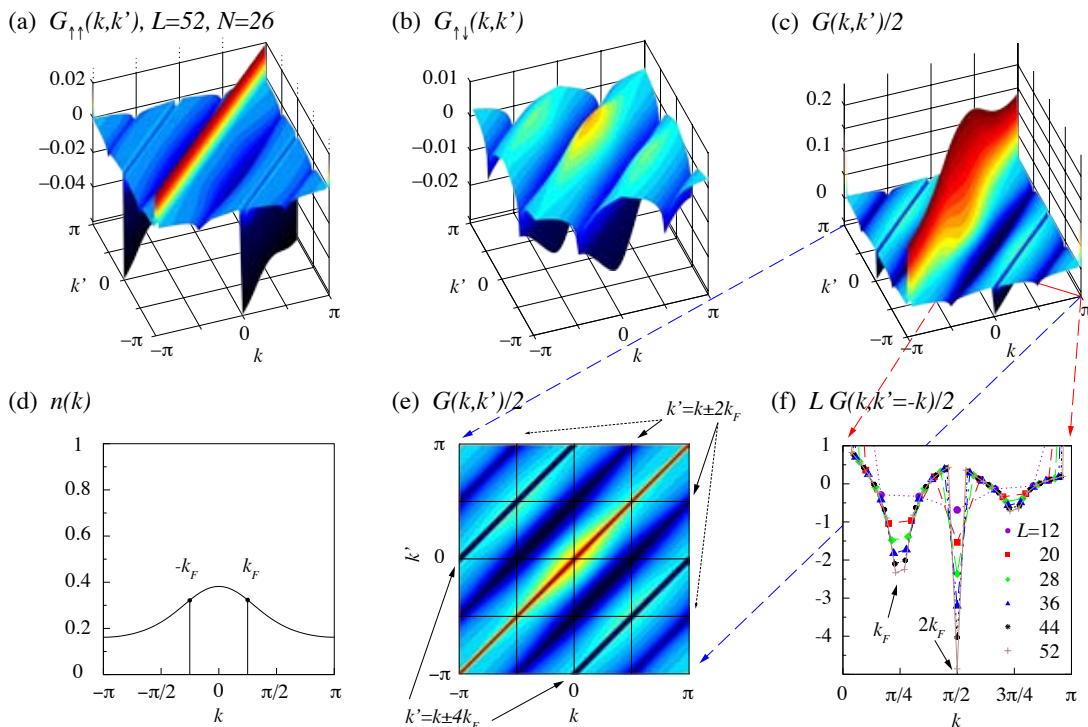


FIG. 4: (Color online). Noise correlations (a, b, c, e, f) and momentum distribution (d) in the extended Hubbard model with $U/t = V/t = 10$ at quarter-filling, i.e., $k_F = \pi/4$. This system is characterized by long-range charge modulations at wave-vector $4k_F$ in $G_{\uparrow\uparrow}$ (a) and algebraically decaying spin-spin fluctuations at $2k_F$ in $G_{\uparrow\uparrow}$ and $G_{\uparrow\downarrow}$ (b). The small dips along $k' = k \pm 3\pi/2$ are simply due to the periodicity of the Brillouin zone. A finite-size scaling analysis of the total shot noise along the anti-diagonal (f) nicely illustrates the difference between true and quasi-long-range order.

sible to bosonization, i.e., around opposing Fermi points, our results for the noise correlations agree well with the behavior illustrated in the last column of Fig. 3 of Ref. 17. Note, however, that the sum rule (5) leads to nonsingular structures in $G_{\uparrow\downarrow}$. Such structures can be clearly seen in Fig. 5(f) as pronounced dips along $k = \pm k_F$. These dips and valleys are necessary to compensate the strong positive contributions due to the singlet superconducting correlations and are not predicted by bosonization.

F. Metallic Tomonaga-Luttinger liquid

We take the conventional repulsive Hubbard model at filling $x = 3/8$ with $U/t = 10$ as an example of a spin-1/2 Luttinger liquid with both gapless charge and spin excitations. From Refs. 24, 34, we estimate $K_\rho \approx 0.58$, while $K_\sigma = 1$ due to the $SU(2)$ symmetry. According to Refs. 25, 33, the density-density and spin-spin correlations decay with the same exponent $1 + K_\rho$ (neglecting

logarithmic corrections)

$$C_{CDW} = \langle n_l n_0 \rangle \rightarrow n^2 - \frac{K_\rho}{(\pi l)^2} + B_{CDW} \frac{\cos(2k_F l)}{|l|^{K_\rho+1}} + B'_{CDW} \frac{\cos(4k_F l)}{|l|^{4K_\rho}}$$

$$C_{SDW} = \langle S_l^z S_0^z \rangle \rightarrow -\frac{1}{(\pi l)^2} + B_{SDW} \frac{\cos(2k_F l)}{|l|^{K_\rho+1}}, \quad (12a)$$

while the pairing correlations exhibit an unmodulated asymptotic behavior with an exponent $1 + 1/K_\rho$

$$C_{SS} = \langle c_{l,\uparrow}^\dagger c_{l,\downarrow}^\dagger c_{0,\downarrow} c_{0,\uparrow} \rangle \rightarrow \frac{B_{SS}}{|l|^{1/K_\rho+1}}$$

$$C_{TS} = \langle c_{l+1,\downarrow}^\dagger c_{l,\downarrow}^\dagger c_{0,\downarrow} c_{1,\downarrow} \rangle \rightarrow \frac{B_{TS}}{|l|^{1/K_\rho+1}}. \quad (12b)$$

The amplitudes A_ξ, B_ξ depend also on the interactions and on the filling. The shot noise obtained from this system is shown in Fig. 6. In contrast to the previous examples of insulating phases, the momentum distribution [Fig. 6(d)] now has an infinite slope singularity at $q = k_F$, as is characteristic of a TL liquid [35]. This pronounced feature can also be recognized in the noise correlations around the Fermi points, even for strong interaction strength. Although particle-hole fluctuations (which

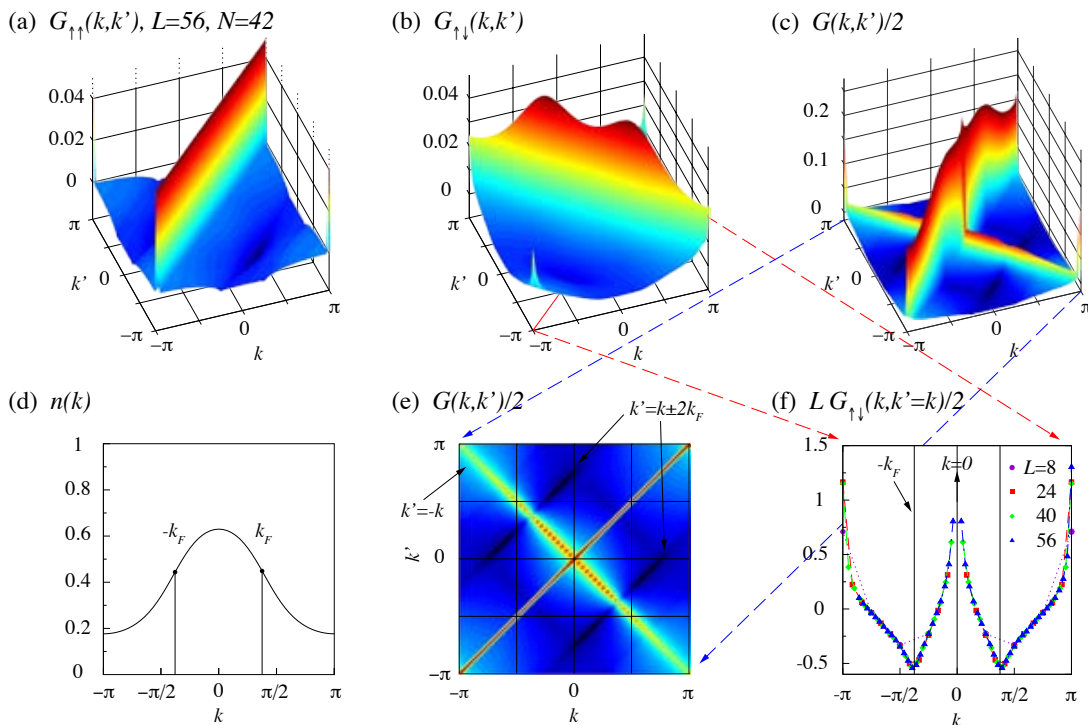


FIG. 5: (Color online). Noise correlations (a, b, c, e, f) and momentum distribution (d) in the attractive Hubbard chain with $U/t = -10$ ($V = 0$) at filling $x = 3/8$. In real space, electrons tend to form coherent on-site singlets. In momentum space, this pairing is reflected in dominant particle-particle correlations along $k = -k'$ in $G_{\uparrow\downarrow}$ (b). In the total shot noise (f), it becomes apparent that the $2k_F$ -CDW fluctuations present in $G_{\uparrow\uparrow}$ (a) are decaying faster than the superconducting fluctuations. In contrast to the noise correlations, the momentum distribution (d) does not reveal any information on the ordering tendencies. Note in (f) the presence of a kink-like negative feature at $\pm k_F$, which compensates the positive response of the pairing correlations, by virtue of the sum rule (5).

are always negative) are dominant for all cases of repulsive interactions, we expect pairing correlations (with positive contributions) to be visible as well, but with a weaker dependence on the system size. Our numerical results confirm these expectations: In $G_{\uparrow\uparrow}$, Fig. 6(a) and $G_{\uparrow\downarrow}$, Fig. 6(b), the dips along $k' = k \pm 2k_F$ are well-pronounced, whereas the particle-particle peaks close to the Fermi points are barely discernible. It is interesting to note that the main features describing this metallic phase already emerge from a simple perturbative calculation; see appendix A and compare with Fig 7. The behavior around opposing Fermi points ($k = k_F$, $k' = -k_F$) is in perfect qualitative agreement with recent bosonization results [Eq. (8) of Ref. 17]. The detection of $4k_F$ charge fluctuations, which are present in principle, is hindered by the fact that they decay as a power law with an exponent significantly larger than two and presumably have a small amplitude A'_{CDW} .

G. Summary

Let us now summarize the main signatures of different phases that can be observed in the noise correlations. As a general rule, particle-particle fluctuations give a

TABLE II: Diverging behavior observed in the rescaled noise correlations LG for different phases. A plus (+) or minus (-) symbol indicates the sign of the singularity.

Phase	$LG_{\uparrow\uparrow}$	$LG_{\uparrow\downarrow}$
Charge-density wave (CDW)	-	0
Spin-density wave (SDW)	-	-
Singlet superconductivity (SS)	0	+
Triplet Superconductivity (TS)	+	+
Bond-order wave (BOW) / dimerization	-	0

positive contribution and are observed along the anti-diagonal $k' = -k$ of the shot noise, while particle-hole correlations enter with a negative sign and lead to dips along $k' = k \pm q$. The strong signal along the diagonal $k' = k$ contains only information that is already encoded in the momentum distribution. Tab. II summarizes the five different phases encountered in the examples presented above, indicating the sign of the singularities in the rescaled noise correlations LG , together with the channels in which they can be observed. If there is only one ordering tendency in the system, it can be identified unambiguously. However, as soon as there are two or more competing phases, one has to include additional information to distinguish between them.

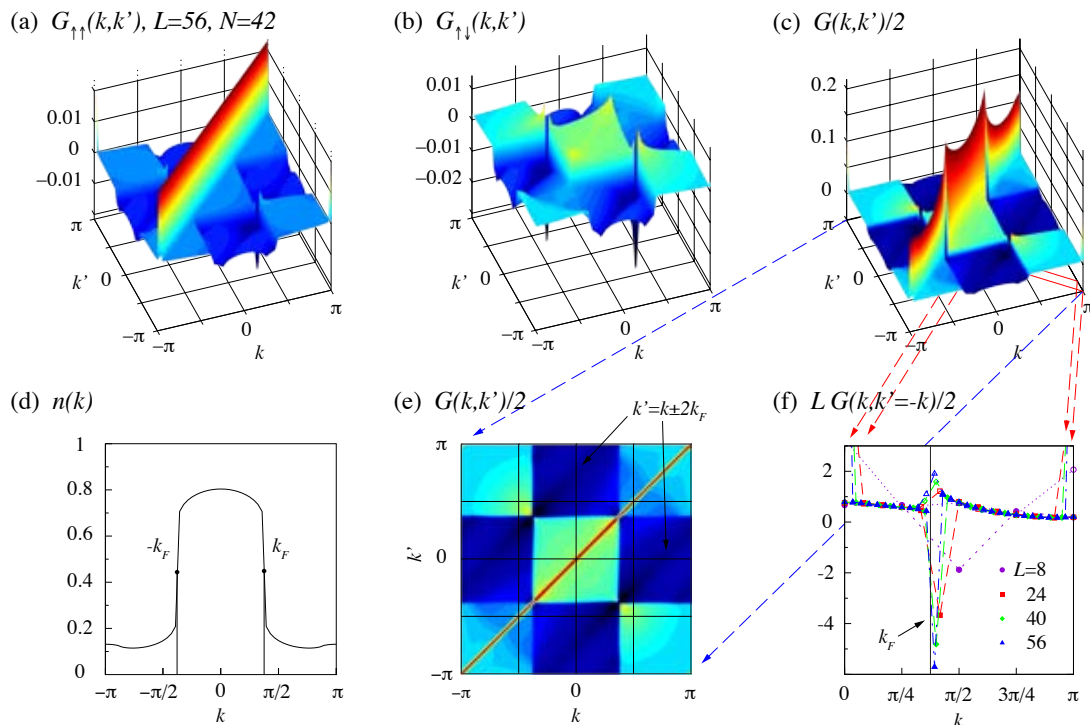


FIG. 6: (Color online). Noise correlations (a, b, c, e, f) and momentum distribution (d) in the Hubbard model in a metallic phase with $U/t = 10$ ($V = 0$) at filling $x = 3/8$. The metallic character is reflected by the infinite slope (not jump) singularity of the momentum distribution (d) at $k = \pm k_F$. This singularity also translates itself to the noise correlations. CDW and SDW signatures (with a negative sign, due to their particle-hole nature) are recognizable along $k' = k \pm 2k_F$, while the small positive peaks around the Fermi points are due to the pairing fluctuations. The chosen parameters correspond to a Luttinger liquid correlation exponent $K_\rho \approx 0.58$.

V. EXPERIMENTAL CONSIDERATIONS

Finally, we would like to put these numerical results in context with respect to experiments. Initially, the atoms would be confined in an optical lattice. By using PBC in our numerical calculations, we have neglected the presence of a shallow confining potential as well as the open ends of the 1D system. We have tested the sensitivity of the shot noise to the choice of boundary conditions in the case of a combined CDW/SDW; see Sec. IV D. Qualitatively, we find exactly the same features for OPC as for PBC, namely, a pronounced dip along $k' = k \pm 4k_F$ in $G_{\uparrow\uparrow}$, indicating the presence of a CDW, and a less distinct valley along $k' = k \pm 2k_F$ in $G_{\uparrow\uparrow}$ and $G_{\uparrow\downarrow}$, reflecting the SDW ordering (not shown). After the trap is turned off, the atom cloud expands freely, allowing the momentum distribution $n_\sigma(k)$ as well as the noise correlations $G_{\sigma\sigma'}(k, k')$ to be measured. The relationship between the freely expanding atom cloud and the initial lattice states of the trapped atoms is explained in detail in Ref. 11. We are thus confident that our results directly apply to experimental realizations and measurements. The summary of features present in the noise correlations (Tab. II) clearly illustrates the necessity for state-selective measurements to distinguish different phases, as the sign of the signal reveals only the character of the

fluctuation, i.e., particle-hole- or particle-particle-like.

VI. CONCLUSION

We have analyzed the noise correlations (density-density correlations in momentum space) in various phases of the extended Hubbard model in one dimension. Our numerical density-matrix renormalization group study, carried out for several characteristic interactions and fillings, shows that different types of (quasi-)long-range order leave different fingerprints in the shot noise. This allows different phases to be identified and distinguished with a universal probe. The method is therefore of interest for experiments with ultracold atoms, in which the shot noise can be extracted from time-of-flight images. We have also pointed out the importance of sum rules, i.e., the fact that the integral over the Brillouin zone is equal to zero, which leads to the interesting effect that noise features due to correlations must be compensated by a (possibly nonsingular) complementary structure. In the future, it would be desirable to obtain similar ab-initio results for the noise correlations of various fermionic systems in two dimensions, notably the repulsive Hubbard model at and away from half filling. Furthermore the effect of finite temperature

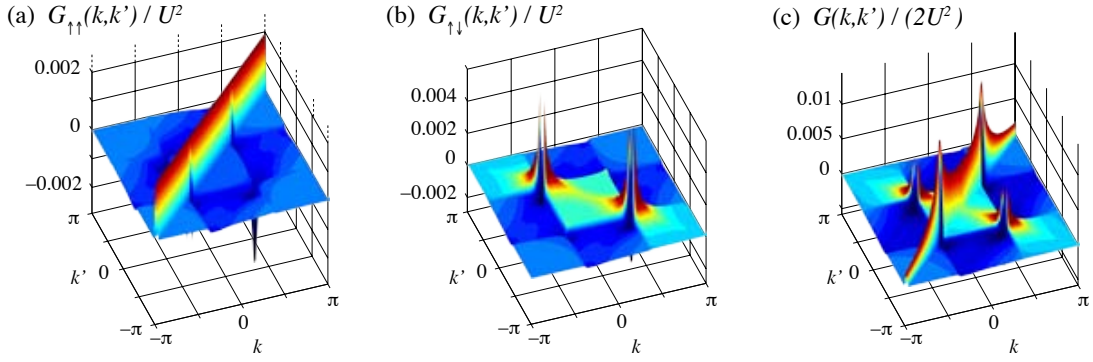


FIG. 7: (Color online). Noise correlations G/U^2 obtained in second-order perturbation theory for a metallic system at a filling of $x = 3/8$. When compared to the DMRG results shown in Fig. 6, the positive peaks in the vicinity of opposite Fermi points due to particle-particle correlations are more pronounced. The analytical expressions have been evaluated here for $L = 56$ and $N = 42$.

on the noise profiles needs to be investigated.

Acknowledgments

We are grateful to O. Sushkov and T. Giamarchi for valuable discussion. This work was supported by the Swiss National Science Foundation. The ED calculations were performed on the Cray XT3 at CSCS (Manno, Switzerland). One of us (A.M.L.) acknowledges the warm hospitality of the School of Physics at UNSW (Sydney, Australia) during his stay in the final stage of the project.

APPENDIX A: PERTURBATIVE REGIME

For $t' = V = 0$ and small on-site interactions $|U| \ll 1$, one can calculate the noise correlations in perturbation theory. In the momentum representation, the Hamiltonian (10) reads

$$H = \sum_{k,\sigma} \epsilon_k c_{k,\sigma}^\dagger c_{k,\sigma} - \frac{U}{L} \sum_{\substack{k,k',q \\ k \neq k'}} c_{k,\uparrow}^\dagger c_{k',\downarrow}^\dagger c_{q,\uparrow} c_{k+k'-q,\downarrow}, \quad (\text{A1})$$

with the dispersion

$$\epsilon_k = -2 \cos k + 2 \cos k_F \quad (\text{A2})$$

and Fermi momentum $k_F = x\pi$. To first order, the ground state wave function is given by

$$|\Psi\rangle = |F\rangle + \frac{U}{L} \sum_{\substack{k,k',q \\ k \neq k'}} \frac{c_{k,\uparrow}^\dagger c_{k',\downarrow}^\dagger c_{q,\uparrow} c_{k+k'-q,\downarrow}}{\epsilon_k + \epsilon_{k'} - \epsilon_q - \epsilon_{k+k'-q}} |F\rangle, \quad (\text{A3})$$

where $|F\rangle = \prod_{k \leq k_F} c_{k,\sigma}^\dagger |0\rangle$ is the Fermi sea.

1. Momentum distribution

At zero temperature, the momentum distribution of the noninteracting system reads

$$n_\sigma^{(0)}(k) = f(k) = \theta(|k| - k_F),$$

where $\theta(k)$ is the unit step function. For convenience, we also define $\bar{f}(k) = 1 - f(k)$. The first corrections arise in second order perturbation theory and are therefore independent of the sign of U

$$n_\sigma^{(2)}(k) \approx n_\sigma^{(0)}(k) + U^2 [I_1(k) - I_2(k)], \quad (\text{A4})$$

with

$$I_1(k) = \frac{\bar{f}(k)}{L^2} \sum_{\substack{k',q \\ q \neq k}} \frac{\bar{f}(k') f(q) f(k+k'-q)}{(\epsilon_k + \epsilon_{k'} - \epsilon_q - \epsilon_{k+k'-q})^2}$$

$$I_2(k) = \frac{f(k)}{L^2} \sum_{\substack{k',q \\ q \neq k}} \frac{\bar{f}(k') \bar{f}(q) f(k'+q-k)}{(\epsilon_{k'} + \epsilon_q - \epsilon_k - \epsilon_{k'+q-k})^2}.$$

2. Noise correlations

For *non-interacting* fermions on a chain with PBC, $G_{\sigma\sigma'}(k, k') \equiv 0$ because $n_{k,\sigma}$ commutes with the tight-binding Hamiltonian. Analogous to the momentum distribution, the lowest order corrections to the noise correlations are quadratic in U and thus also independent of the sign

$$G_{\sigma\sigma'}^{(2)}(k, k') \approx U^2 \begin{cases} \delta_{\sigma,\sigma'} \delta_{k,k'} I_1(k) + (1 - \delta_{\sigma,\sigma'}) I_4(k, k') - I_1(k) I_1(k') & (k > k_F \wedge k' > k_F) \\ -I_3(k, k') + I_1(k) I_2(k') & (k > k_F \wedge k' \leq k_F) \\ \delta_{\sigma,\sigma'} \delta_{k,k'} I_2(k) + (1 - \delta_{\sigma,\sigma'}) I_5(k, k') - I_2(k) I_2(k') & (k \leq k_F \wedge k' \leq k_F) \end{cases} \quad (\text{A5})$$

with the two-point correlations I_j given by

$$I_3(k, k') = \frac{\bar{f}(k) f(k')}{L^2} \sum_q \frac{\bar{f}(q) f(k+q-k')}{(\epsilon_k + \epsilon_q - \epsilon_{k'} - \epsilon_{k+q-k'})^2},$$

$$I_4(k, k') = \frac{\bar{f}(k) \bar{f}(k')}{L^2} \sum_q \frac{f(q) f(k+k'-q)}{(\epsilon_k + \epsilon_{k'} - \epsilon_q - \epsilon_{k+k'-q})^2},$$

$$I_5(k, k') = \frac{f(k) f(k')}{L^2} \sum_q \frac{\bar{f}(q) \bar{f}(k+k'-q)}{(\epsilon_k + \epsilon_{k+k'-q} - \epsilon_k - \epsilon_{k'})^2}.$$

The normalized noise correlations G/U^2 obtained in this perturbation calculation are shown in Figs. 7 for a metallic system at filling $x = 3/8$. Compared to the DMRG results shown in Fig. 6, the positive peaks in the vicinity of opposite Fermi points due to particle-particle correlations are more pronounced, but, otherwise, the perturbative approach leads to a surprisingly accurate description of the shot noise.

-
- [1] I. Bloch, *Nature Physics* **1**, 23 (2005).
 - [2] D. Jaksch, P. Zoller, *Ann. Phys.* **315**, 52 (2005).
 - [3] O. Morsch and M. Oberthaler, *Rev. Mod. Phys.* **78**, 179 (2006).
 - [4] M. Lewenstein, A. Sanpera, V. Ahufinger, B. Damski, A. Sen De, U. Sen, *Adv. Phys.*, **56**, 243 (2007).
 - [5] I. Bloch, J. Dalibard, and W. Zwerger, arXiv:0704.3011, (unpublished).
 - [6] M. J. Hartmann, F. G. S. L. Brandao, and M. B. Plenio, *Nature Physics* **2**, 849 (2006); D. G. Angelakis, M. F. Santos, and S. Bose, arXiv:quant-ph/0606159 (unpublished); A. D. Greentree, C. Tahan, J. H. Cole, and L. C. L. Hollenberg, *Nature Physics* **2**, 856 (2006).
 - [7] M. Greiner, O. Mandel, T. Esslinger, T. W. Hänsch, and I. Bloch, *Nature (London)* **415**, 39 (2002).
 - [8] T. Stöferle, H. Moritz, C. Schori, M. Köhl, and T. Esslinger, *Phys. Rev. Lett.* **92**, 130403 (2004).
 - [9] K. M. O'Hara, S. L. Hemmer, M. E. Gehm, S. R. Granade, J. E. Thomas, *Science* **298**, 2179 (2002).
 - [10] S. Ospelkaus, C. Ospelkaus, O. Wille, M. Succo, P. Ernst, K. Sengstock, and K. Bongs, *Phys. Rev. Lett.* **96**, 180403 (2006); C. Ospelkaus, S. Ospelkaus, L. Humbert, P. Ernst, K. Sengstock, and K. Bongs, *Phys. Rev. Lett.* **97**, 120402 (2006); for a theoretical analysis of mixtures, see A. Albus, F. Illuminati, and J. Eisert, *Phys. Rev. A* **68**, 023606 (2003); F. Illuminati and A. Albus, *Phys. Rev. Lett.* **93**, 090406 (2004).
 - [11] E. Altman, E. Demler, and M. D. Lukin, *Phys. Rev. A* **70**, 013603 (2004).
 - [12] R. Roth and K. Burnett, *Phys. Rev. A* **67**, 031602(R) (2003).
 - [13] S. Fölling, F. Gerbier, A. Widera, O. Mandel, T. Gericke, and I. Bloch, *Nature* **434**, 481(2005).
 - [14] I.B. Spielman, W.D. Phillips, and J.V. Porto, cond-mat/0606216 (unpublished).
 - [15] M. Greiner, C. A. Regal, J. T. Stewart, and D. S. Jin, *Phys. Rev. Lett.* **94** 110401 (2005).
 - [16] T. Rom, Th. Best, D. van Oosten, U. Schneider, S. Fölling, B. Paredes, and I. Bloch, *Nature* **444**, 733 (2006).
 - [17] L. Mathey, E. Altman, and A. Vishwanath, cond-mat/0507108 (unpublished).
 - [18] S. R.White, *Phys. Rev. Lett.* **69**, 2863 (1992); *Phys. Rev. B* **48**, 10345 (1993).
 - [19] U. Schollwöck, *Rev. Mod. Phys.* **77**, 259 (2005).
 - [20] C. Nayak, *Phys. Rev. B* **62**, 4880 (2000).
 - [21] R. Casalbuoni and G. Nardulli, *Rev. Mod. Phys.* **76**, 263 (2004).
 - [22] T. Giamarchi, *Quantum Physics in One Dimension*, Oxford University Press (2003).
 - [23] N. M. Bogolyubov and V. E. Korepin, *Theoretical and Mathematical Physics* **82**, 231 (1990).
 - [24] H.J. Schulz, *Phys. Rev. Lett.* **64**, 2831 (1990).
 - [25] H. Frahm and V.E. Korepin, *Phys. Rev. B* **42**, 10553 (1990).
 - [26] F. Mila and X. Zotos, *Europhys. Lett.* **24**, 133 (1993).
 - [27] K. Penc and F. Mila, *Phys. Rev. B* **49**, 9670 (1994).
 - [28] S. Daul and R. M. Noack, *Phys. Rev. B* **58**, 2635 (1998).
 - [29] S. Daul and R. M. Noack, *Phys. Rev. B* **61**, 1646 (2000).
 - [30] A. Läuchli, C. Honerkamp, and T. M. Rice, *Phys. Rev. Lett.* **92**, 037006 (2004).
 - [31] C. K. Majumdar and D. P. Ghosh, *J. Math. Phys.* **10**, 1388 (1969).
 - [32] J. Voit, *Rep. Prog. Phys.* **57**, 977 (1994).
 - [33] T. Giamarchi and H. J. Schulz, *Phys. Rev. B* **39**, 4620 (1989).
 - [34] S. Ejima, F. Gebhard, and S. Nishimoto, *Europhys. Lett.* **70**, 492 (2005).
 - [35] M. Ogata and H. Shiba, *Phys. Rev. B*, **41**, 2326 (1990).